
Masters Theses

Student Theses and Dissertations

Summer 2024

Branching Fractional Brownian Motion

Reece Beattie-Hauser

Missouri University of Science and Technology

Follow this and additional works at: https://scholarsmine.mst.edu/masters_theses



Part of the [Physics Commons](#)

Department:

Recommended Citation

Beattie-Hauser, Reece, "Branching Fractional Brownian Motion" (2024). *Masters Theses*. 8199.
https://scholarsmine.mst.edu/masters_theses/8199

This thesis is brought to you by Scholars' Mine, a service of the Missouri S&T Library and Learning Resources. This work is protected by U. S. Copyright Law. Unauthorized use including reproduction for redistribution requires the permission of the copyright holder. For more information, please contact scholarsmine@mst.edu.

BRANCHING FRACTIONAL BROWNIAN MOTION

by

REECE BEATTIE-HAUSER

A THESIS

Presented to the Graduate Faculty of the

MISSOURI UNIVERSITY OF SCIENCE AND TECHNOLOGY

In Partial Fulfillment of the Requirements for the Degree

MASTER OF SCIENCE

in

PHYSICS

2024

Approved by:

Thomas Vojta, Advisor
Alexey Yamilov
Aleksandr Chernatynskiy

ABSTRACT

Fractional Brownian Motion (FBM) is a Gaussian process whose increments are correlated over long times. FBM is an example of anomalous diffusion, and recently it has been used to model the distribution of serotonergic fibers in the brain [1, 2]. To better represent these fibers, branching FBM (bFBM), where FBM trajectories may randomly split into two, is introduced. One-dimensional bFBM is studied in both subdiffusive and superdiffusive regimes, examining three potential behaviors of the correlations (memory) in a branching event: both trajectories retain the memory of previous steps, only one keeps the memory, and neither keeps the memory. Trajectories' mean-square displacements are calculated, as well as the mean-square separation and step correlations between pairs of branching trajectories, and found to be in good agreement with theoretical predictions. Branching FBM's qualitative features' strong dependence on memory behavior is confirmed.

ACKNOWLEDGMENTS

I would like to thank my advisor, Thomas Vojta, for his years of continued support, guidance, and patience. His teaching has been a powerful force in both advancing my understanding and in shaping my career.

I would like to thank the other members of my committee, Alexey Yamilov and Aleksandr Chernatynskiy, for lending me their time and for their words of encouragement.

I would like to thank Gaurav Khairnar for his collaboration in developing and optimizing the implementation of the Hosking algorithm used in this work, as well as for the several enlightening discussions we have had about our research.

I would like to thank Jonathan House, whose work — though not reported here — forms the cornerstone of the research my group has done on branching fractional Brownian motion. I would also like to thank Angela Rayle, who is currently assembling our group's work on branching fractional Brownian motion into a manuscript for publication.

I would like to thank Skirmantas Janušonis and Ralf Metzler, whose collaboration with Thomas Vojta motivated the research done here. Without them, this work would not have been possible.

I would also thank my family for their unwavering support and company.

This work was supported in part by the National Science Foundation under Grants No. IIS-2112862 and No. OAC-1919789, and by the Cottrell SEED award from Research Corporation.

TABLE OF CONTENTS

	Page
ABSTRACT	iii
ACKNOWLEDGMENTS	iv
LIST OF ILLUSTRATIONS	vi
 SECTION	
1. INTRODUCTION.....	1
2. REVIEW OF FRACTIONAL BROWNIAN MOTION	3
2.1. NORMAL DIFFUSION AND BROWNIAN MOTION	3
2.2. ANOMALOUS DIFFUSION AND FRACTIONAL BROWNIAN MOTION	6
3. BRANCHING FRACTIONAL BROWNIAN MOTION	13
3.1. MONTE CARLO SIMULATION.....	16
3.2. RESULTS	19
4. CONCLUSIONS	26
 APPENDICES	
A. PROOF OF THE SELF-SIMILARITY OF FRACTIONAL BROWNIAN MOTION	28
B. MEAN SQUARED SEPARATION OF BRANCHING TRAJECTORIES	32
C. STEP CORRELATIONS AFTER BRANCHING IN NO-LOSS MODEL	36
REFERENCES	40
VITA.....	42

LIST OF ILLUSTRATIONS

Figure	Page
1.1. Side-by-side comparison of serotonergic fibers and FBM trajectories demonstrating their similarity	2
1.2. Image showing the branching of a serotonergic fiber, originally published in Ref. [3].....	2
3.1. Comparison of the MSD of a parent-child trajectory pair following a branch in the no-loss, half-loss, and full-loss models.....	20
3.2. Comparison of the MSS of a parent-child trajectory pair following a branch in the no-loss and full-loss models	21
3.3. The percent difference between fitted and theoretical values of the MSS coefficient as a function of the branch time t_b	22
3.4. Correlations between simultaneous steps of parent and child trajectories following a branch in the no-loss model	23
3.5. Comparison of the MSD in the no-loss, half-loss, and full-loss models with a constant branching rate of $\lambda_b = 0.01$	25

1. INTRODUCTION

The brains of all vertebrate animals are permeated by a dense network of neuron axons that release the neurotransmitter serotonin. These serotonergic axons (also called fibers) belong to cells whose bodies reside in a number of brainstem clusters known as the raphe nuclei [2]. Much is known about the impact these fibers have on the brain; for instance, perturbations to the density of this fiber network have been associated with Major Depressive Disorder and epilepsy [4, 5]. Unfortunately, very little is known about how the network develops. However, it has recently been suggested that the growth of these fibers is actually a stochastic process [6]. Specifically, these fibers appear to behave in a way similar to a process known as fractional Brownian motion (FBM) [2].

Fractional Brownian motion is a generalization of the better-known Brownian motion, which is a model of normal diffusion. In contrast, FBM can be used to model diffusive behavior not described by Brownian motion, known as anomalous diffusion. Anomalous diffusion comes in two varieties, namely superdiffusion and subdiffusion, which, as the names imply, refer to processes that disperse *more* quickly or *less* quickly (respectively) than normal diffusion.

As previously mentioned, FBM has seen significant success as a model of the growth of serotonergic axons, particularly superdiffusive FBM. Superficially, the paths traced by FBM bear significant resemblance to the individual fibers (see Fig. 1.1), but far more convincing is the rigorous statistical analysis of the resultant steady-state densities of superdiffusive FBM that found quantitative agreement with the densities of fibers in the brain [2, 7].

Despite FBM's success as a model of these fibers, there are still areas where it can be refined. There are several fundamental differences between FBM and the fibers it models. For instance, serotonergic fibers have been observed to occasionally branch (see

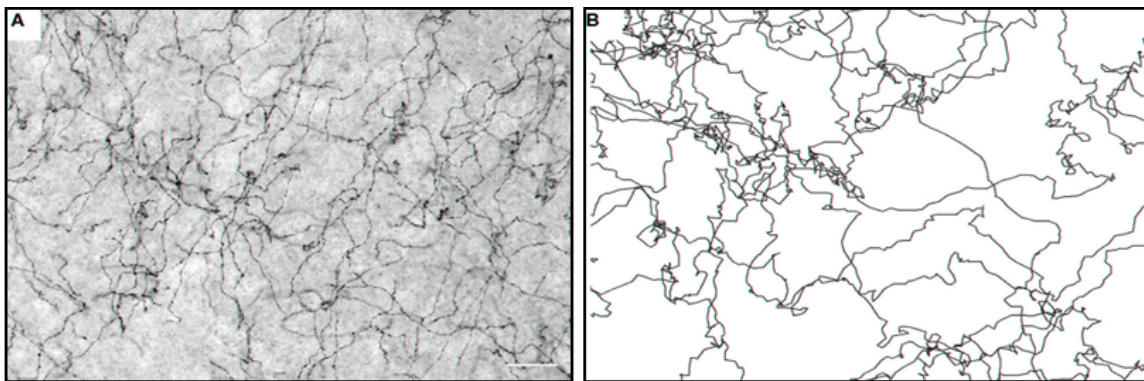


Figure 1.1. Side-by-side comparison of serotonergic fibers and FBM trajectories demonstrating their similarity. Figure taken with permission from Ref. [2]. (A) 40 μm -thick cross section of mouse brain with serotonergic fibers highlighted in black. (B) Simulated superdiffusive FBM sample trajectories ($\alpha = 1.6$).

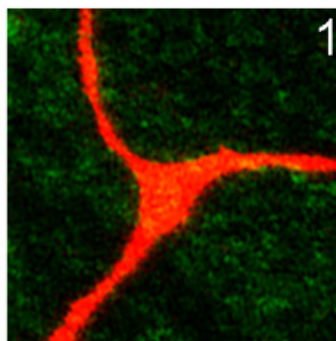


Figure 1.2. Image showing the branching of a serotonergic fiber, originally published in Ref. [3]. The area pictured is about 9.5 μm by 9.5 μm .

Fig.1.2), there being no such mechanism in FBM. To better represent the real fibers, the model of branching fractional Brownian motion (bFBM) is introduced. In this thesis, a basic definition of bFBM is constructed and many of its basic properties are studied.

2. REVIEW OF FRACTIONAL BROWNIAN MOTION

2.1. NORMAL DIFFUSION AND BROWNIAN MOTION

Brownian motion is a type of uncorrelated random movement. The increments of the motion (or steps, as they will often be referred to as in this paper) are Gaussian-distributed — that is, the individual displacements experienced over the course of a motion occur with probabilities according to a Gaussian distribution. The process is named for Robert Brown, who first observed the phenomenon in pollen particles in 1828 [8], but it was arguably Einstein [9] who popularized the topic and whose work would form the foundation of the subject for years to come. In cases like those recorded by Brown, the motion is caused by the interaction between the particles and the medium they reside in. Brown's pollen particles were much lighter than the water they were suspended in, and so the erratic thermal motion of the water molecules could accelerate the particles significantly. To an observer, the resultant motion appears highly random.

A mathematical definition of Brownian motion can be constructed just from the basic description given above. The position x_B at time t (given that the motion begins at $t = 0$) can be defined as the integral¹

$$x_B(t) = \int_0^t \xi_B(s) ds, \quad (2.1)$$

where ξ_B are the increments of the motion (sometimes called Gaussian noise or white noise). These increments are Gaussian-distributed random numbers with zero mean. The increments are uncorrelated, which can be expressed as

$$\langle \xi_B(s) \xi_B(t) \rangle = \sigma^2 \delta(s - t), \quad (2.2)$$

¹Note that stochastic integrals like in Eq. (2.1) are not generally Riemann integrable [10]. Stochastic calculus is a deep mathematical field, but with some caution, many of the complications of evaluating stochastic integrals are avoided in this paper without needing to refer to the techniques of stochastic calculus.

where the angle brackets denote an ensemble average, σ^2 is the variance of the distribution, and δ is the Dirac- δ function.

It is now possible to derive a few important results, even only with these relatively basic definitions. First, the mean displacement of the particle is, trivially,

$$\begin{aligned}\langle x_B(t) \rangle &= \int_0^t \langle \xi_B(s) \rangle ds \\ &= 0,\end{aligned}\tag{2.3}$$

due to the increments having zero mean ($\langle \xi_B(t) \rangle = 0$). However, the mean *squared* displacement (MSD) is

$$\begin{aligned}\langle x_B^2(t) \rangle &= \iint_0^t \langle \xi_B(s) \xi_B(s') \rangle ds' ds \\ &= \iint_0^t \sigma^2 \delta(s - s') ds' ds \\ &= \sigma^2 \int_0^t ds \\ &= \sigma^2 t.\end{aligned}\tag{2.4}$$

This result, implying that the MSD grows linearly with time, is the distinguishing characteristic of *normal diffusion*.

Let us now consider the probability density of Brownian motion when the particle is confined to some finite interval. Without needing to refer to mathematics, one can reasonably assume that the particle will be equally likely to be found anywhere inside the interval after a significant amount of time has passed since the particle was released from its starting point. It is well known that normal diffusion results in a uniform distribution when it reaches a steady state, so considering that Brownian motion is a mechanism for normal diffusion, the natural conclusion is that the probability distribution becomes flat after a long time has passed. Hence, the particle being contained within a finite interval — without a boundary, the MSD will continue to increase forever and the system will never reach a

steady state. Given that Brownian motion is uncorrelated over long times, the particle will eventually “forget” its starting position, and since the particle has no preference of direction or location, it is intuitively clear that the particle’s probability density will be uniformly distributed over the interval. The uniform distribution of steady-state normal diffusion is another one of its key properties, though it is not unique to normal diffusion. Compare this to heat dissipation. Given the fluctuation-dissipation theorem is fulfilled, the system will eventually reach thermal equilibrium and heat will be spread evenly through the available space. Even if the system is briefly perturbed, the system will eventually return to thermal equilibrium. Brownian motion also fulfills the fluctuation-dissipation theorem [11], thus a system of particles performing Brownian motion eventually reach equilibrium and become evenly spread throughout their container, and even if this were to be perturbed (by adding or subtracting particles to or from a particular location, for instance), the particles would eventually return to equilibrium and again uniformly fill their container.

The requirements for random motion to qualify as normal diffusion (which is contrasted with *anomalous diffusion* in Sec. 2.2) are that the motion be local in time and space. In other words, the motion is uncorrelated beyond a well-defined time scale and the increments possess a well-defined length scale [12]. Both of these are clearly satisfied by Brownian motion as defined in Eqs. (2.1) and (2.2)²: the increments are perfectly uncorrelated in time and the length scale is defined by σ^2 .

One may find the requirements for normal diffusion to be too restrictive; it is not difficult to construct a process that violates one or both of these requirements. For example, consider a random motion whose steps have a power law distribution (a process known as a Lévy flight [12]). Depending on the choice of parameters, the mean step length may diverge and give the motion an ill-defined length scale, so this clearly would not qualify as normal diffusion. Another way to violate the requirements for normal diffusion is to construct a

²It should be noted that this is not the only way to construct Brownian motion mathematically, as the only requirements are that it be an uncorrelated, Gaussian process. For instance, the increment correlations could be defined by exponential decay instead of by the Dirac- δ , which would still fulfill the requirement that the correlations be local in time.

process that is non-Markovian. A Markovian process is one that can be evolved from one state to the next using only the information about the current state. Brownian motion is a Markovian process; the state of Brownian motion is described completely by the current position, and the next position is found by simply adding some random increment. A non-Markovian process may depend not just on the current state, but also the state before, or maybe the state before that, etc. — i.e., non-Markovian processes have *memory*. One such example of a non-Markovian, random motion is FBM, which is discussed in the following section.

2.2. ANOMALOUS DIFFUSION AND FRACTIONAL BROWNIAN MOTION

As described at the end of the previous section, random motion is not necessarily local in time and space. Such motion that does not fit within the definition of normal diffusion is referred to as *anomalous diffusion*. Anomalous diffusion differs from normal diffusion in several easily observable ways, such as the MSD, which follows the power law

$$\langle x^2(t) \rangle = K_\alpha t^\alpha, \quad (2.5)$$

where α and K_α are the anomalous diffusion exponent and anomalous diffusion coefficient associated with the process in question [12]. The exponent α can be used to characterize how quickly a process diffuses, and is often used to divide anomalous diffusion into two broad categories: subdiffusion and superdiffusion. Subdiffusive processes have $0 < \alpha < 1$ and thus diffuse more slowly than normal diffusion, with a limiting case at $\alpha = 0$, where particles never leave the local “neighborhood” around their starting position, possibly corresponding to harmonic motion or simply non-motion. Superdiffusive processes have $\alpha > 1$ and thus diffuse more quickly than normal diffusion, and while $\alpha = 2$ (i.e. ballistic motion) may be

a limiting case for many superdiffusive processes (FBM included, as demonstrated later in this section), it is not required to be. For instance, for particular choices of parameters, Lévy flights may have a divergent MSD and thus diffuse more quickly than ballistic motion³.

Additionally, anomalous diffusion does not necessarily share normal diffusion's uniform probability distribution in a steady state. In particular, FBM has been observed to result in probability densities with strong biases near the boundaries [13, 14]. Specifically, superdiffusive FBM trajectories tend to accumulate at the boundary while subdiffusive trajectories accumulate away from the boundary, the latter effect being referred to as depletion.

Before discussing the macroscopic details, however, a proper introduction of FBM is in order. Fractional Brownian motion is largely identical to Brownian motion (both are Gaussian processes with stationary increments), except the increments in FBM have slowly decaying correlations that lack a well-defined time scale. A process similar to FBM was described by Lévy in 1953 [15] using the integral

$$x(t) = K_L \int_0^t (t-s)^{H-1/2} \xi_B(s) ds, \quad (2.6)$$

where K_L is a constant, ξ_B are Brownian increments as described in Sec. 2.1 and H is the Hurst parameter, limited to $0 < H < 1$ and here corresponding to how strongly the increments are correlated. Note that a Hurst parameter value of $H = 1/2$ recovers the definition of Brownian motion given in Eq. 2.1. This definition yields an MSD of

$$\begin{aligned} \langle x^2(t) \rangle &= K_L^2 \iint_0^t (t-s)^{H-1/2} (t-s')^{H-1/2} \langle \xi_B(s) \xi_B(s') \rangle ds' ds \\ &= K_L^2 \iint_0^t (t-s)^{H-1/2} (t-s')^{H-1/2} \delta(s-s') ds' ds \\ &= K_L^2 \int_0^t (t-s)^{2H-1} ds \\ &= \frac{1}{2H} K_L^2 t^{2H}. \end{aligned} \quad (2.7)$$

³While it is true that the mathematical construction of Lévy flights allow for superballistic motion, it should be noted that no physical process can be asymptotically superballistic, as they are eventually limited by the finite speed of light.

This result gives the value of α for FBM:

$$\alpha = 2H, \quad (2.8)$$

and $0 < H < 1$, so $0 < \alpha < 2$, which makes ballistic motion the limiting case of superdiffusive FBM.

Mandelbrot and van Ness, building off of the work of Kolmogorov [16], completed the definition of FBM by iterating on Lévy's description, as they felt it put "too great an importance on the origin" [17]. They addressed this issue by having FBM formally start at $t = -\infty$:

$$\begin{aligned} x(t) &= K_M \left[\int_{-\infty}^t (t-s)^{H-1/2} \xi_B(s) ds - \int_{-\infty}^0 (-s)^{H-1/2} \xi_B(s) ds \right] \\ &= K_M \left\{ \int_0^t (t-s)^{H-1/2} \xi_B(s) ds + \int_{-\infty}^0 \left[(t-s)^{H-1/2} - (-s)^{H-1/2} \right] \xi_B(s) ds \right\}, \end{aligned} \quad (2.9)$$

where K_M is a constant. A natural consequence of this revised definition is that the increments $x(t) - x(\tau)$ are now *stationary*. That is, a trajectory can be defined with respect to any fixed time without affecting its evolution. Eq. 2.9 is defined with respect to $t = 0$, but it would be equally valid to define it relative to $t = 10^8$.

Calculating the MSD is somewhat less obvious than with the process Lévy described, so it will be performed once again:

$$\begin{aligned} \langle x^2(t) \rangle &= K_M^2 \left\{ \iint_0^t (t-s)^{H-1/2} (t-s')^{H-1/2} \delta(s-s') ds' ds \right. \\ &\quad \left. + \iint_{-\infty}^0 \left[(t-s)^{H-1/2} - (-s)^{H-1/2} \right] \left[(t-s')^{H-1/2} - (-s')^{H-1/2} \right] \delta(s-s') ds' ds \right\} \\ &= K_M^2 \left\{ \int_0^t (t-s)^{2H-1} ds + \int_{-\infty}^0 \left[(t-s)^{H-1/2} - (-s)^{H-1/2} \right]^2 ds \right\}. \end{aligned}$$

Note that the cross terms can be ignored because the bounds for each integral do not overlap. Now, the first integral can be carried out the same as in Eq. 2.7, and substituting $u = s/t$ in the second integral and factoring out the resulting t gives

$$\begin{aligned}\langle x^2(t) \rangle &= K_M^2 \left\{ \frac{t^{2H}}{2H} + t^{2H} \int_{-\infty}^0 \left[(1-u)^{H-1/2} - (-u)^{H-1/2} \right]^2 du \right\} \\ &= K_M^2 \left\{ \frac{1}{2H} + \int_{-\infty}^0 \left[(1-u)^{H-1/2} - (-u)^{H-1/2} \right]^2 du \right\} t^{2H} \\ &= K_\alpha t^\alpha,\end{aligned}\tag{2.10}$$

which differs from Eq. 2.7 only by a constant factor.

The MSD is time-translation invariant, meaning $\langle [x(\tau+t) - x(\tau)]^2 \rangle = \langle x^2(t) \rangle$, making it trivial to show that FBM's covariance is

$$\langle x(t)x(\tau) \rangle = \frac{1}{2} K_\alpha (t^\alpha - |t - \tau|^\alpha + \tau^\alpha),\tag{2.11}$$

which can be used to derive the correlation between increments. But first, let the increments in continuous-time FBM be defined as

$$\xi(t) = x(t + \delta t) - x(t),\tag{2.12}$$

where $\delta t > 0$ is constant⁴. Making use of Eq. (2.11), the increments' correlations⁵ are

$$\langle \xi(\tau)\xi(\tau+t) \rangle = \frac{1}{2} K_\alpha [|t + \delta t|^\alpha - 2t^\alpha + |t - \delta t|^\alpha].\tag{2.13}$$

⁴While in FBM, we may choose δt (also called the lag time) to be constant, physical systems often have a distribution of varying lag times. However, if the distribution of lag times is sufficiently narrow (e.g. Gaussian) and does not change as the motion evolves, then we can assume that the lag times for two steps are, on average, approximately equal. So while there is no mathematical issue in assuming that δt is constant, this assumption is not likely to cause any issues when modeling physical systems using FBM. Also, allowing the lag times of the two steps in Eq. 2.13 to be different does not significantly impact the result, as the correlations will still be stationary and behave the same in the long-time limit.

⁵Strictly speaking, Eq. (2.13) is the increments' covariance, not their correlations. However, if the increments have unit variance (as is often assumed in the literature and in this paper), the covariance and correlations are equal due to the increments having zero mean.

Note that the correlations depend only on the time between steps t and not on τ , meaning the correlations are stationary. It is not intuitively clear how this function behaves over time, but consider its behavior when $t \gg \delta t$. Taylor expanding to second order about $\delta t = 0$ yields the approximate form

$$\begin{aligned} \langle \xi(\tau)\xi(\tau+t) \rangle &\approx \frac{1}{2}K_\alpha \delta t^2 \alpha(\alpha-1)t^{\alpha-2} \\ &= \frac{1}{2}K_\alpha \delta t^2 \alpha(\alpha-1)t^{-\gamma}, \end{aligned} \tag{2.14}$$

where $\gamma = 2 - \alpha$ is the FBM correlation exponent. Since $0 < \gamma < 2$, the correlations must decay as a power law. This behavior gives FBM a long memory, thus making the process non-Markovian and violating the requirements for normal diffusion. Also note the prefactor of $\alpha - 1$, which implies that the increments are *positively* correlated for $\alpha > 1$ (superdiffusive) and *negatively* correlated for $\alpha < 1$ (subdiffusive). This means superdiffusive FBM is more likely to move in the same direction repeatedly, while subdiffusive FBM is more likely to move in the direction opposite its previous movement.

Mandelbrot and van Ness' formulation of FBM is powerful and reveals much information about the process, but it is unwieldy for any non-trivial use. There is no closed form for Eq. 2.9, so it often cannot be used analytically. The only other option then is to use numerics, but the lower integration bound of $s = -\infty$ makes this inconvenient. One could use Lévy's FBM-like process and evaluate Eq. 2.6 with quadrature, but the white noise signal ξ_B is poorly behaved, which makes many methods ineffective. However, being a Gaussian process, FBM is fully described by its covariance. This means that any process with the correct covariance, continuous or discrete, can produce FBM. As such, the best solution — in the author's opinion — is to find a discrete FBM process (rather than an integral approximation), which is generally much easier to handle numerically.

Qian [18] introduced a discretization of FBM that is a sum of a fractional Gaussian noise, which has components ξ :

$$x_t = \xi_1 + \xi_2 + \cdots + \xi_t, \quad (2.15)$$

for positive integer t . They defined a fractional Gaussian noise as a series of Gaussian-distributed, random variables ξ with the property

$$\sqrt{\text{Var} [\xi_1 + \xi_2 + \cdots + \xi_N]} = N^H \sqrt{\text{Var} [\xi_1]}, \quad (2.16)$$

meaning the series is self-similar (like FBM itself, as demonstrated in Appendix A). Also note that this is functionally equivalent to Eq. (2.5).

Since the variance of this sum of fractional Gaussian noise depends only on the number of ξ participating in the sum, it thus has the same time-translation invariance as FBM ($\langle (x_t - x_\tau)^2 \rangle = |t - \tau|^{2H} \text{Var}[\xi_1]$), again making it trivial to show that the covariance is

$$\langle x_t x_\tau \rangle = \frac{1}{2} \text{Var} [\xi_1] \left(t^{2H} - |t - \tau|^{2H} + \tau^{2H} \right). \quad (2.17)$$

From Eq. (2.16), it is clear that $\text{Var}[\xi_1] = K_\alpha$, and therefore this covariance is exactly Eq. (2.11). This confirms that this discrete process produces FBM (with lag time $\delta t = 1$, given that the increments are $\xi_t = x_t - x_{t-1}$).

Now having obtained a discretization, all that remains to be able to simulate FBM is to find a source of fractional Gaussian noise. One available method is the Fourier filtering algorithm of Makse et al. [19], which, as the name implies, produces fractional Gaussian noise by performing a series of Fourier transforms on an input set of random data. First, an input set of Gaussian random numbers is transformed into Fourier space, then multiplied with the square root of the Fourier transform of the correlation function in Eq. (2.13). This product is then inverse Fourier transformed back to real space, the result of which is a set of

Gaussian random numbers with the desired correlations. This method has its advantages, as fast Fourier transform algorithms are quite efficient, but it also has its drawbacks. Most importantly, because every component of the output relies on every component of the input, the Fourier filtering algorithm does not allow for any sort of intervention in the produced noise without destroying the correlations between steps. If it was necessary to change one of the output ξ , one would have to regenerate the entire set.

An alternative method is the Hosking algorithm [20], which generates the fractional Gaussian noise iteratively — something the Fourier filtering algorithm cannot do. This is very useful for simulating branching FBM (as discussed in Sec. 3), as it gives us the freedom to reuse steps, allowing two FBM trajectories to share memory. The Hosking algorithm's downside, however, is that it has a relatively large computational complexity of $O(N^2)$, N being the desired number of steps in a trajectory. The Fourier filtering method (and all fast Fourier transform algorithms), by comparison, has complexity $O(N \log N)$.

3. BRANCHING FRACTIONAL BROWNIAN MOTION

With the definition of FBM and its properties established, it is now time to introduce the concept of branching. Some aspects of branching FBM (bFBM) have already been studied in mathematical literature [21, 22], though they are largely concerned with properties different from those studied in this paper.

As discussed in Sec. 2.2, the defining characteristic of FBM is that the process has **memory**. If FBM trajectories are allowed to branch, how should their memory behave after branching? Should the two trajectories share the memory from before the branch? Should the memory from before the branch decay more quickly? While there are any number of complex possibilities for the memory behavior, here we will study three very simple all-or-nothing models, where a trajectory either keeps all the memory from before a branch or loses all the memory. The models will be called *no-loss*, *half-loss*, and *full-loss*¹. In the no-loss model, both trajectories will keep the memory from before the branch; in the half-loss model, only one of the trajectories will keep the memory from before the branch; and in the full-loss model, neither trajectory will keep the memory from before the branch.

Because these models are relatively simple, we can already begin to draw conclusions about how they will behave. For instance, consider the MSD of two trajectories that branched from each other at a time $t = t_b$. The MSD following the branch is then

$$\langle x^2(t > t_b) \rangle = \frac{1}{2} [\langle x_p^2(t) \rangle + \langle x_c^2(t) \rangle], \quad (3.1)$$

¹Strictly speaking, FBM cannot lose memory. Per the Mandelbrot-van Ness definition, all FBM starts at minus infinity. Rather, it would be more accurate to describe a branch event as an intersection between two trajectories at a particular time. In the no-loss model, the two trajectories have the same history for times before the branch; they are two different valid realizations of FBM for a given history. In the half-loss model, the “child” is an independent trajectory that intersects the “parent” at the branch. Aside from that intersection, they are completely unrelated. In the full-loss model, the original trajectory ends at the branch and two other independent trajectories intersect where it ended, one of which “replaces” the original trajectory. However, because the increments are stationary, the existence of infinitely-long memory (or lack thereof) has no practical effect on the collective behavior. For this reason, memory “loss” following a branch is modeled as a true loss of memory.

where x_p and x_c are the positions of the parent and child trajectories, respectively. There should not be any effect on the MSD in the no-loss model as both trajectories' correlations are unchanged. In the half-loss and full-loss models, however, the two trajectories are uncorrelated to each other. Trajectories that have lost the memory of their history can be conceptualized as FBM trajectories that have been translated to start at time $t = t_b$ and position $x = x_b$. In the half-loss model, the parent trajectory is unaffected by the branch while the child trajectory loses the memory from before the branch, so their MSDs are

$$\left. \begin{aligned} \langle x_p^2(t) \rangle &= K_\alpha t^\alpha \\ \langle x_c^2(t) \rangle &= K_\alpha [(t - t_b)^\alpha + t_b^\alpha] \end{aligned} \right\} \quad (\text{half-loss model}). \quad (3.2)$$

The MSD averaged between the two is then

$$\langle x^2(t > t_b) \rangle = \frac{1}{2} K_\alpha [t^\alpha + (t - t_b)^\alpha + t_b^\alpha] \quad (\text{half-loss model}). \quad (3.3)$$

In the full-loss model, however, x_p has also lost the memory, so the MSDs are then

$$\left. \begin{aligned} \langle x_p^2(t) \rangle &= K_\alpha [t_b^\alpha + (t - t_b)^\alpha] \\ \langle x_c^2(t) \rangle &= K_\alpha [t_b^\alpha + (t - t_b)^\alpha] \end{aligned} \right\} \quad (\text{full-loss model}), \quad (3.4)$$

so the overall MSD is

$$\langle x^2(t > t_b) \rangle = K_\alpha [(t - t_b)^\alpha + t_b^\alpha] \quad (\text{full-loss model}). \quad (3.5)$$

These analytical results are compared to numerical simulation data in Sec. 3.2. In addition, the mean squared separation (MSS) between two trajectories that branched from one another can be found in closed form for the half-loss and full-loss models. The behavior of the MSS in the no-loss model, however, is non-trivial, as the two trajectories remain correlated to each other following the branch, and these unknown correlations make the problem intractable in

discrete-time bFBM. Though there is an exact solution for the MSS in the no-loss model in continuous-time bFBM (see Appendix B), it is not entirely clear if it holds in discrete-time bFBM. The result for the continuous-time MSS in the no-loss model is compared to the discrete-time simulation data in Sec. 3.2.

Now consider the MSD when trajectories branch at a constant rate λ_b , referred to as the branching rate. The number of trajectories N will increase exponentially over time, like

$$N(t) \propto e^{\lambda_b t}. \quad (3.6)$$

This is not expected to have any effect on the MSD in the no-loss model, as in the case of a single branch. In the half-loss and full-loss models, however, this means that trajectories that are uncorrelated from their histories are being added at an exponential rate. As a result, the system begins to cross over into an uncorrelated regime at $t \approx 1/\lambda_b$, when young trajectories begin to outnumber older trajectories. Given that FBM's long-time correlations are the sole characteristic distinguishing FBM from Brownian motion (and the origin of FBM's anomalous diffusion character), the expectation is then that this uncorrelated regime will exhibit Brownian-like behavior. For the MSD, this corresponds to a crossover to linear behavior, as in Eq. (2.4). Both the half-loss and full-loss models are expected to cross over to Brownian-like behavior, but the full-loss model is expected to cross over more quickly than the half-loss model, as the full-loss model not only adds uncorrelated trajectories but also destroys the correlations of existing trajectories. The crossover is still expected to start at $t \approx 1/\lambda_b$, but the transition should take less time to complete.

3.1. MONTE CARLO SIMULATION

This study reports the results of simulations of one-dimensional branching FBM (bFBM) in free space, though all of the results discussed in Sec. 3.2 can be generalized to higher dimensions with little issue. A d -dimensional FBM process is equivalent to d independent 1-dimensional FBM processes evolving in parallel [1], so introducing additional degrees of freedom will not meaningfully impact the qualitative behavior observed.

In the simulation, the FBM steps were generated using the Hosking algorithm [20], with input random numbers from Marsaglia's 2005 KISS random number generator [23]. The Hosking algorithm is used here as it allows trajectories to share memory with one another, as described near the end of Sec. 2.2. The step lengths are generated with unit variance, which means — as implied by Eq. (2.16) — the anomalous diffusion coefficient is $K_\alpha = 1$.

Branching FBM has a tree-like structure. For this study, the initial state of bFBM is considered to be a single particle which may branch into more particles as the system evolves. The trajectory of the initial particle is the root of the tree structure, and each branching event creates two leaves. In the case of a constant branching rate, a trajectory may branch with probability λ_b at each time step, and the average number of trajectories in a tree will grow like in Eq. (3.6). This exponential growth of the number of trajectories over time is very computationally expensive. To combat this, the simulation allows trajectories to decay (i.e. terminate) at a rate of λ_d per time step (where λ_d is called the decay rate), where — after decaying — trajectories no longer contribute to any data collected. The decay rate, combined with the branching rate, causes the number of trajectories to behave like

$$\langle N(t) \rangle = e^{(\lambda_b - \lambda_d)t}, \quad (3.7)$$

which is averaged over the total number of trees being sampled. Allowing trajectories to decay is not expected to affect the macroscopic behavior of bFBM, as its only effect is to decrease the number of trajectories without affecting those that survive.

Even while allowing trajectories to decay at a rate λ_d , the branching of trajectories and sharing of memory still presents a significant computational problem. As per Eq. (3.7), the number of trajectories increases exponentially over time. The problem is then that the computer memory required to store the trajectories' histories will quickly exceed that available for the simulation. One might expect this to severely limit the maximum time scale that can be reasonably simulated, and while it is true that the exponentially increasing number of trajectories does put significant limitations on the number of time steps that can be reasonably simulated, this is not due to the amount of computer memory required for the simulation. In fact, a simulation of N_t time steps only needs to store N_t integers in addition to the data needed to simulate a single trajectory. This relatively efficient use of memory is possible due to an algorithm that makes use of the fact that the trajectories are non-interacting, which is detailed below.

The algorithm functions primarily through the use of a stack of trajectories' start times. Each time a branching event occurs, the time at which it occurred is placed at the top of the stack. Because the trajectories are non-interacting, only one trajectory needs to be considered at a time (rather than simulating all trajectories simultaneously). In addition, any information that will not be remembered by a trajectory's children (i.e. information from after they branched from their parent) can be discarded after the trajectory has reached the end of the simulation. Each time the program finishes simulating a trajectory, the simulation is repeated starting from the time at the top of the stack (while also removing this time from the stack) until the stack is empty. Given that a trajectory can only branch once per time step, the stack will have a maximum of N_t elements in the worst-case scenario where a trajectory branches on every time step.

The aforementioned algorithm for simulating an entire tree of trajectories while efficiently sharing trajectory memory is as follows:

1. Initialize a stack of start times containing only the start time of the initial trajectory
2. Get the start time at the top of the stack and pop it off the the stack
3. Simulate an FBM trajectory (that may or may not reuse the history of its parent trajectory, if any) from the start time retrieved in the previous step until a specified end time, putting the times of any branching events the trajectory encounters at the top of the stack, and overwriting the post-branch history of the parent trajectory (if any) with the current trajectory's history
4. Gather data about the completed trajectory
5. Repeat steps 2 through 4 until the stack of start times is empty

The simulation estimates the ensemble average of a quantity A at time t by

$$\langle A(t) \rangle = \frac{1}{N_{trees}(t)} \sum_{i=1}^{N_{trees}} \langle A(t) \rangle_i, \quad (3.8)$$

where N_{trees} is the number of trees being sampled² and $\langle A(t) \rangle_i$ is the mean of $A(t)$ in tree i , defined as

$$\langle A(t) \rangle_i = \frac{1}{N_i(t)} \sum_{j=1}^{N_i(t)} A_{ij}(t), \quad (3.9)$$

where $N_i(t)$ is the number of trajectories in tree i at time t and $A_{ij}(t)$ is the value of the quantity A belonging to trajectory j of tree i (if $N_i(t) = 0$, however, then $\langle A(t) \rangle_i = 0$ and does not contribute to the ensemble average). In other words, the ensemble average is estimated using an average of averages. First, the average is taken over the trajectories in each tree, then the average is taken over trees.

²The number of trees being sampled decreases over time due to trajectory decay, as trees will sometimes decay more quickly than they branch. It should be noted that Eq. (3.7) is unique in that the average is with respect to the initial number of trees being sampled and not the number of trees remaining at time t .

Normal FBM is characterized by the strength of the correlations between its increments, determined by the Hurst parameter H . This is still true in bFBM, but the relationship between H and the different observable parameters may change. It is therefore important to distinguish the input parameters from those that are observed. For the remainder of this paper, the FBM correlation exponent $\gamma = 2 - 2H$, introduced in Eq. (2.14), will refer to the correlations of the input fractional Gaussian noise, while α will refer only to the observed exponent of the MSD.

The simulations that used a fixed branching time gathered data from 10^5 to 3×10^7 trees, depending on the sensitivity to noise of the desired quantities. However, simulations allowing random branching sampled data from only 9000 to 12000 trees, being much more computationally expensive and the data being gathered also being generally less sensitive to noise.

The branching and decay rates were chosen to be $\lambda_b = 0.01$ and $\lambda_d = 0.009$. These rates are close in value in order to mitigate the effect of an exponentially increasing number of trajectories due to branching. It is also important to avoid $\lambda_b < \lambda_d$, as it severely limits the trajectories' lifetimes in which to demonstrate their behavior. Therefore, a difference of rates is chosen to be $\lambda_b - \lambda_d = 0.001$, the magnitudes of λ_b and λ_d being selected arbitrarily.

To evenly distribute the computational workload between compute nodes, the simulation program uses the multifit job scheduling algorithm of Coffman, Garey, and Johnson [24]. This is done because the number of trajectories in a particular tree can vary greatly between trees, so two different trees can require vastly different amounts of computational effort to simulate.

3.2. RESULTS

The expectations for the MSD of a parent-child trajectory pair in the half-loss and full-loss models are given in Eqs. (3.3) and (3.5). Figure 3.1 compares these to simulation data, demonstrating good agreement between them. The expectation that a single branch

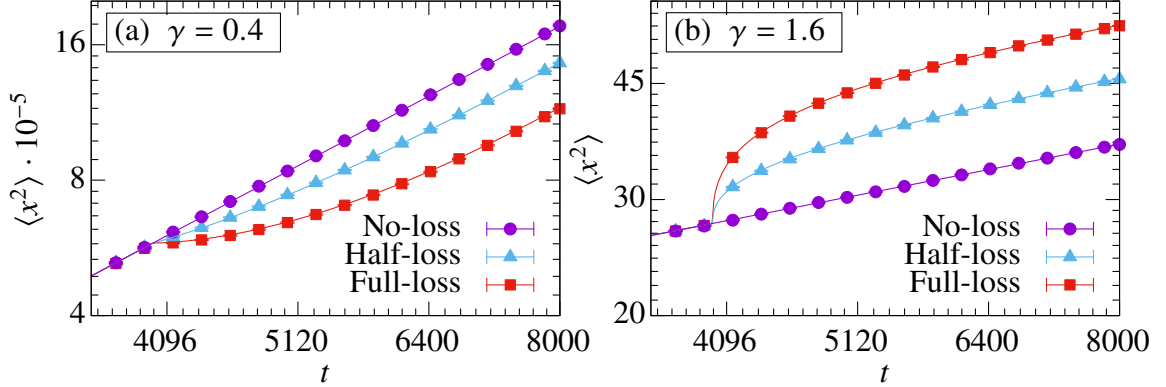


Figure 3.1. Comparison of the MSD of a parent-child trajectory pair following a branch in the no-loss, half-loss, and full-loss models. Solid lines through no-loss, half-loss, and full-loss data are Eqs. (2.5), (3.3), and (3.5), respectively, with the coefficient set to $K_\alpha = 1$ and the exponent set to $\alpha = 2 - \gamma$. Branch time is fixed at $t_b = 4000$. (a) Superdiffusive case, $\gamma = 0.4$. (b) Subdiffusive case, $\gamma = 1.6$.

event does not effect the MSD in the no-loss model is also confirmed. This result gives a basic illustration of the effect of memory loss. It demonstrates the deviations from the typical $t^{2-\gamma}$ behavior of FBM, and how the magnitude of these deviations also depend on if whether one or both branching trajectories lose memory.

The MSS of a parent-child trajectory pair is derived for the half-loss and full-loss models in Appendix B. Figure 3.2 demonstrates the agreement between the expected results and the simulation data, as well as the differing results for the no-loss model. Visual inspection of the no-loss data (as well as numerical fits to a power law) imply that they follow the same exponent $\alpha = 2 - \gamma$ as the half-loss and full-loss data, only with a different constant prefactor. This agrees with the theoretical result for the no-loss model's MSS

$$\begin{aligned} \langle \Delta x^2(t) \rangle &= K_\alpha (t - t_b)^{2H} \frac{2^{2H} \sqrt{\pi}}{\Gamma(1-H)\Gamma(H+1/2)} \\ &= K_s (t - t_b)^{2H} \end{aligned} \quad (3.10)$$

found by Casanova and Igelbrink in their study of continuous-time bFBM [22], where Γ is the gamma function and K_s is a constant, here referred to as the MSS coefficient.

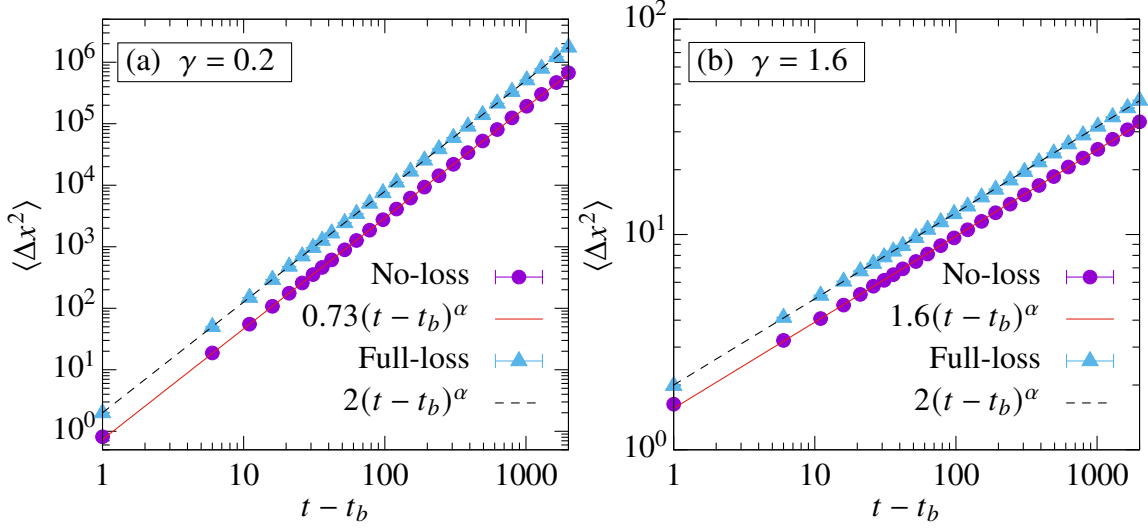


Figure 3.2. Comparison of the MSS of a parent-child trajectory pair following a branch in the no-loss and full-loss models. Results for half-loss model are near-identical to those of the full-loss model. Branch time is fixed at $t_b = 4000$. Solid line is a power-law fit to the no-loss data, where the coefficient is a fit parameter and the exponent is fixed at $\alpha = 2 - \gamma$. Dashed line has a fixed coefficient of 2 and fixed exponent of $\alpha = 2 - \gamma$. (a) Superdiffusive case, $\gamma = 0.2$. (b) Subdiffusive case, $\gamma = 1.6$.

There is some slight disagreement between the exact numerical value of the MSS coefficient resulting from fits of simulation data to Eq. (3.10) and the expected theoretical value of $K_s = K_\alpha 2^{2H} \sqrt{\pi} / \Gamma(1 - H) \Gamma(H + 1/2)$. This could be a discretization effect, but the difference between the theoretical and fitted values of K_s decreases monotonically with increasing branch time t_b (see Fig. 3.3). This suggests that the discrepancy is caused by a fundamental shortcoming of numerical simulations of FBM, which is that simulated trajectories are restricted to having a finite amount of memory. Formally, FBM trajectories have an infinitely long history, per Eq. (2.9). This is not normally an issue when simulating FBM because the increments are stationary; the precise amount of memory a trajectory has is irrelevant as long as memory is never lost. In the case of bFBM, however, limitations of numerical simulations only allow trajectories to share a finite amount of memory when

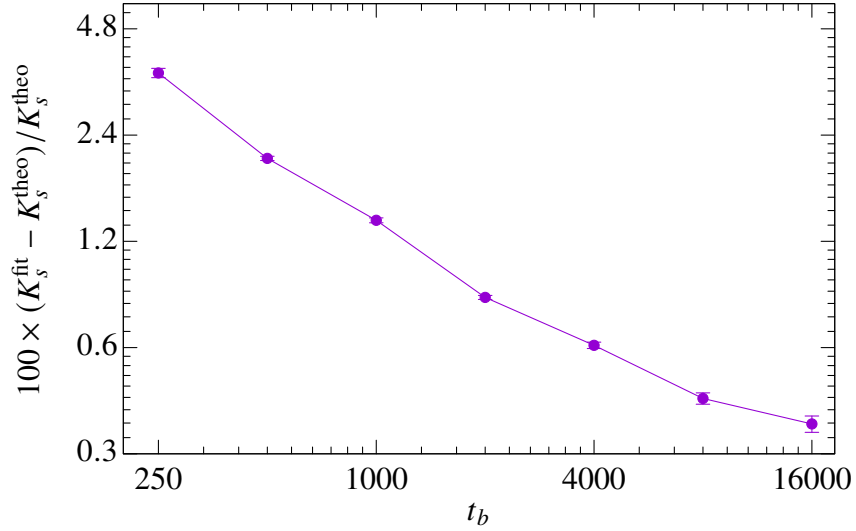


Figure 3.3. The percent difference between the fitted and theoretical values of the MSS coefficient as a function of the branch time t_b . K_s^{fit} is the coefficient resulting from fits of MSS simulation data to Eq. (3.10) with the exponent fixed at $2H = 2 - \gamma$, and K_s^{theo} is the theoretical value listed in Eq. (3.10). Data is for systems with FBM correlation exponent $\gamma = 0.2$ in the no-loss model, where the theoretical value of the MSS coefficient is $K_s \approx 0.7312$.

they *should* share an infinite amount of memory. For this reason — and based on the results shown in Fig. 3.3 — it seems likely that the value of K_s should asymptotically approach its theoretical value as $t_b \rightarrow \infty$.

The results for the no-loss MSS make it clear that the steps of two branching trajectories remain correlated to each other after the branch (see Eq. (7) of Appendix B). A plot of the correlations between simultaneous steps of parent and child trajectories in the no-loss model can be found in Fig. 3.4. Only data for the superdiffusive case is shown, as the subdiffusive step correlation data is extremely erratic and requires sampling a prohibitively large number of trees to achieve good convergence in data averages. Figure 3.4(a) compares the step correlations of different FBM correlation exponents γ . Strikingly, the data suggest that the correlations behave like

$$\langle \xi(t) \xi'(t) \rangle \propto (t - t_b)^{-\gamma} \quad (3.11)$$

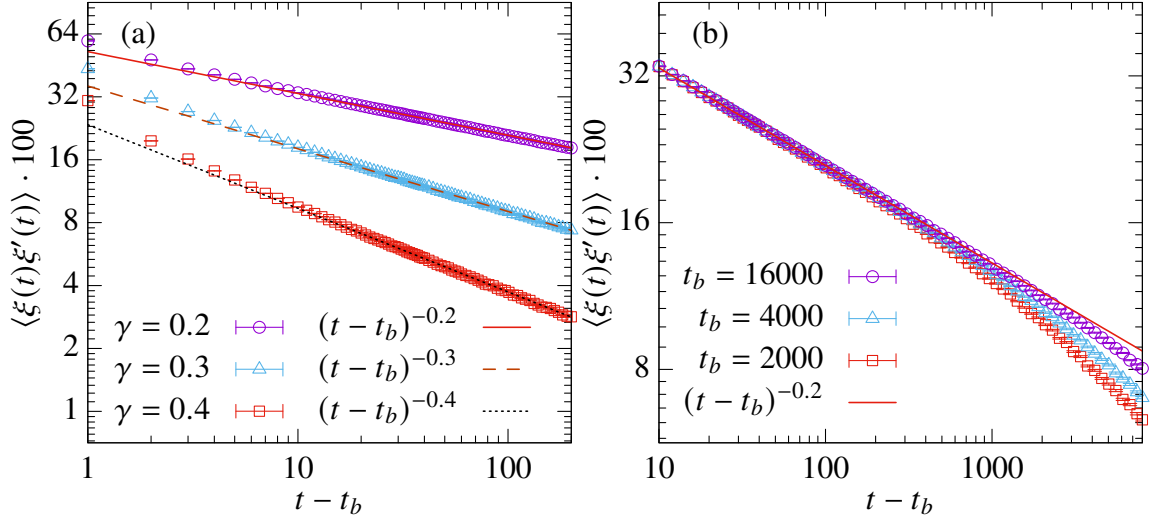


Figure 3.4. Correlations between simultaneous steps of parent and child trajectories following a branch in the no-loss model. (a) Branch time is fixed at $t_b = 8000$. Solid, dashed, and dotted lines are power-law fits to $\gamma = 0.2$, $\gamma = 0.3$, and $\gamma = 0.4$ data (respectively) where the coefficients are fit parameters and the exponents are fixed at $-\gamma$. (b) Correlation exponent is $\gamma = 0.2$; solid line is the same fit as the solid line in panel (a).

for $t - t_b \gtrsim 20$. This aligns with the theoretical result for continuous-time bFBM (see Appendix C), which predicts that the correlations are

$$\begin{aligned} \langle \xi(t)\xi'(t) \rangle &\approx (t - t_b)^{2H-2} \frac{2^{2H}(H - 1/2)\sqrt{\pi}}{(2H - 2)\Gamma(-H)\Gamma(H - 1/2)} \\ &= K_c(t - t_b)^{-\gamma}, \end{aligned} \quad (3.12)$$

where K_c is a constant, here referred to as the step correlation coefficient.

The coefficients of the fits in Fig. 3.4(a) are $K_c \approx 0.5265$, $K_c \approx 0.3603$, and $K_c \approx 0.2346$ for $\gamma = 0.2$, $\gamma = 0.3$, and $\gamma = 0.4$, respectively. These are in reasonably good agreement with their theoretical values, differing at most by 8%. In addition, the agreement is moderately better for larger t_b , similar to the case with the MSS coefficient. It is also to be expected that the fitted and theoretical values differ more than with the MSS coefficient, as Eq. (3.12) is only an approximate form while Eq. (3.10) is an exact result.

However, as can be seen in Fig. 3.4(b), Eq. (3.11) does not hold at sufficiently large t . However, the time where the correlations $\langle \xi(t)\xi'(t) \rangle$ begin to diverge from Eq. (3.11) increases for larger values of t_b — i.e. when the trajectories have a longer shared history. Similar to the discrepancy between the fitted and theoretical values of the MSS coefficient K_s , this suggests that in “true” FBM, where trajectories have infinite histories, Eq. (3.11) would hold for all $t > t_b$.

As previously discussed, allowing trajectories to branch at a constant rate is expected to cause a crossover to an uncorrelated, Brownian-like regime in the half-loss and full-loss models, though the no-loss model should not experience any macroscopic changes. Specifically, in the half-loss and no-loss models, the MSD is expected to transition from normal FBM behavior ($\alpha = 2 - \gamma$) to Brownian behavior ($\alpha = 1$) at $t \approx 1/\lambda_b$. These expectations are confirmed by the simulation data for the MSD, graphs of which can be found in Fig. 3.5. Also, as expected, the full-loss model finishes crossing over to Brownian motion slightly more quickly than the half-loss model.

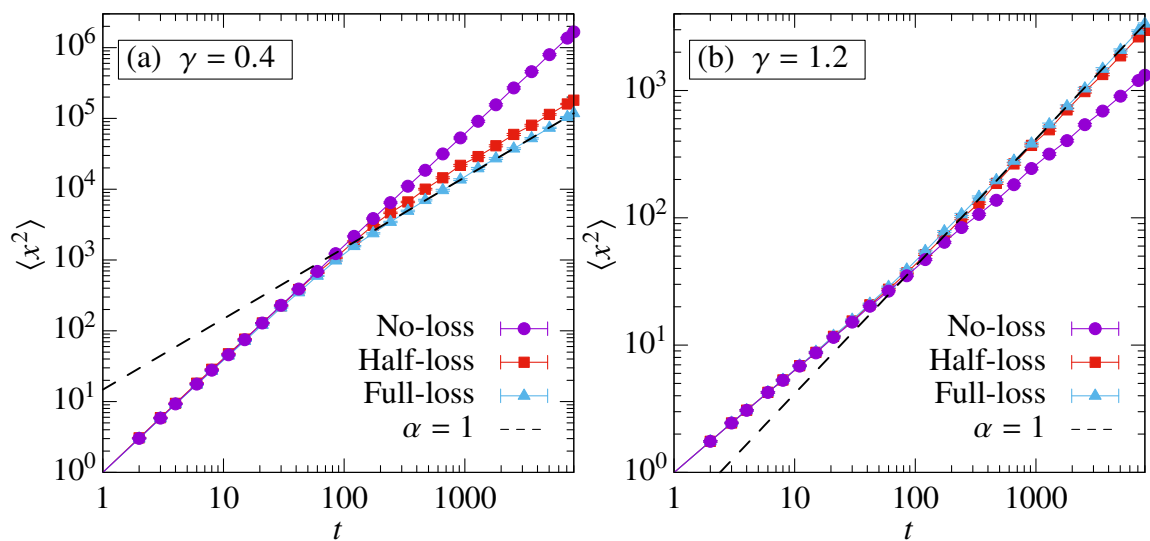


Figure 3.5. Comparison of the MSD in the no-loss, half-loss, and full-loss models with a constant branching rate of $\lambda_b = 0.01$. Dashed line is a fit of a linear function (i.e. $\alpha = 1$) to the full-loss data after the cross over to Brownian motion ($t > 400$), the slope of the line being the only fit parameter. (a) Superdiffusive case, $\gamma = 0.4$. (b) Subdiffusive case, $\gamma = 1.2$.

4. CONCLUSIONS

In this work, a basic framework for bFBM has been constructed and analyzed. Results of computer simulations of bFBM have generally been found to agree very well with theoretical predictions and expectations. There are slight differences in the precise values of the MSS and step correlation coefficients, K_s and K_c , though these discrepancies are not irresolvable, as they are likely caused by the necessarily finite memory of simulated FBM trajectories. It is expected that these quantities will agree with theoretical predictions in the limit of $t_b \rightarrow \infty$. There is also the inconsistency present in the long term behavior of the step correlations of branching trajectories $\langle \xi(t)\xi'(t) \rangle$ in the no-loss memory model. Per the data in Fig. 3.4(b) and the results derived in Appendix C, however, it is also likely that the correlations of two branching trajectories' steps behave like $\langle \xi(t)\xi'(t) \rangle \propto (t - t_b)^{-\gamma}$ for all $t > t_b$ in the limit of infinite memory.

The only result which has no precise mathematical prediction for its behavior is the MSD (when trajectories branch at a constant rate). Even so, the simulation results do agree with the qualitative expectations, namely that the half-loss and full-loss models begin crossing over to Brownian motion at $t \approx 1/\lambda_b$ while the no-loss model is undisturbed. One may feel that the results demonstrating the correlations between branching trajectories in the no-loss model are in conflict with the conclusion that FBM is undisturbed by branching in the no-loss model, but to the contrary, it is precisely because of these correlations that FBM is undisturbed.

The fact that the MSD remains the same in the presence of branching (given that trajectories keep their memory) is a promising result for FBM as a model of serotonergic fibers. As mentioned in Sec. 1, FBM has seen success as a model of these fibers. These results for the MSD serve as preliminary evidence indicating that FBM is unchanged in the no-loss model of bFBM, supporting the validity of FBM as a model of serotonergic fibers.

The most prominent characteristic of (superdiffusive) FBM making it a compelling model of serotonergic fibers is the statistical agreement between FBM's steady-state densities and the observed densities of serotonergic fibers in mouse brains [2]. Results for the steady-state densities of bFBM are still forthcoming, but the work discussed in this paper has laid the foundation for further study. A publication detailing a more in-depth investigation of bFBM as a model of serotonergic fibers (including analysis of bFBM's steady-state densities) is currently being drafted [25].

Many open questions still remain. There is much that is not known about the serotonergic fibers themselves — for instance, at what rate do serotonergic fibers branch? How strongly are branching fibers correlated to each other? Do the strength of these correlations agree with the expectations from FBM? There are open physics questions as well. How do interactions between FBM trajectories affect their evolution? How strongly or weakly can trajectories interact while maintaining FBM's efficacy as a model? How is the evolution affected further if branching is also included, and are the results compatible with the known characteristics of the fibers?

APPENDIX A.

PROOF OF THE SELF-SIMILARITY OF FRACTIONAL BROWNIAN MOTION

Mandelbrot and van Ness define the increments of a random function to be self-similar to mean they have the property that if they are rescaled along a certain dimension, they may be rescaled along another dimension to recover the original increments [17]:

$$X(\tau + t) - X(\tau) \triangleq h^{-H} [X(\tau + ht) - X(\tau)], \quad (1)$$

for any τ , $h > 0$, and $H > 0$, where the notation $x \triangleq y$ means that random variables x and y have the same distribution functions (i.e. share a state space). It is well known that Brownian motion is self-similar in this way, with parameter $H = 1/2$.

In the Mandelbrot-van Ness definition of FBM, the increments are

$$\begin{aligned} x(\tau + t) - x(\tau) &= K_M \left[\int_{-\infty}^{\tau+t} (\tau + t - s)^{H-1/2} \xi_B(s) ds - \int_{-\infty}^{\tau} (\tau - s)^{H-1/2} \xi_B(s) ds \right] \\ &= K_M \left[\int_{-\infty}^t (t - s)^{H-1/2} \xi_B(s) ds - \int_{-\infty}^0 (-s)^{H-1/2} \xi_B(s) ds \right]. \end{aligned} \quad (2)$$

With time rescaled by constant h , the increments are written

$$x(\tau + ht) - x(\tau) = K_M \left[\int_{-\infty}^{ht} (ht - s)^{H-1/2} \xi_B(s) ds - \int_{-\infty}^0 (-s)^{H-1/2} \xi_B(s) ds \right]. \quad (3)$$

Substituting $u = s/h$ yields

$$\begin{aligned} x(\tau + ht) - x(\tau) &= K_M \left[\int_{-\infty}^t (ht - hu)^{H-1/2} \xi_B(hu)(h du) \right. \\ &\quad \left. - \int_{-\infty}^0 (-hu)^{H-1/2} \xi_B(hu)(h du) \right] \\ &= K_M h^{H+1/2} \left[\int_{-\infty}^t (t - u)^{H-1/2} \xi_B(hu) du - \int_{-\infty}^0 (-u)^{H-1/2} \xi_B(hu) du \right]. \end{aligned} \quad (4)$$

As previously stated, Brownian motion is self-similar, meaning

$$x_B(\tau + t) - x_B(\tau) \triangleq h^{-H} [x_B(\tau + ht) - x_B(\tau)]. \quad (5)$$

By the definition of Brownian motion (Eq. 2.1), the increments are the time derivative of the motion:

$$\xi_B(t) = \frac{d}{dt}x_B(t), \quad (6)$$

given $x_B(0) = 0$. By the limit definition of the derivative, the increments can be written

$$\begin{aligned} \xi_B(t) &= \lim_{\delta t \rightarrow 0} \frac{x_B(t + \delta t) - x_B(t)}{\delta t} \\ &\triangleq \lim_{\delta t \rightarrow 0} h^{-1/2} \frac{x_B(t + h \delta t) - x_B(t)}{\delta t} \\ &= \lim_{\delta t \rightarrow 0} h^{1/2} \frac{x_B(t + h \delta t) - x_B(t)}{h \delta t}. \end{aligned} \quad (7)$$

Being a stationary process, the increments of Brownian motion are invariant under translations of the reference time (which is t inside the limit), so

$$x_B(t + h \delta t) - x_B(t) \triangleq x_B(ht + h \delta t) - x_B(ht). \quad (8)$$

Therefore, the relationship between Brownian motion's scaled and unscaled increments can be found by rewriting the above as

$$\begin{aligned} \xi_B(t) &\triangleq h^{1/2} \lim_{\delta t \rightarrow 0} \frac{x_B(ht + h \delta t) - x_B(ht)}{h \delta t} \\ &= h^{1/2} \frac{d}{d(ht)} x_B(ht) \\ &= h^{1/2} \xi_B(ht). \end{aligned} \quad (9)$$

Plugging this result into Eq. 4 yields

$$\begin{aligned}
 x(\tau + ht) - x(\tau) &\triangleq K_M h^{H+1/2} \left\{ \int_{-\infty}^t (t-u)^{H-1/2} \left[h^{-1/2} \xi_B(u) \right] du \right. \\
 &\quad \left. - \int_{-\infty}^0 (-u)^{H-1/2} \left[h^{-1/2} \xi_B(u) \right] du \right\} \\
 &= K_M h^H \left[\int_{-\infty}^t (t-u)^{H-1/2} \xi_B(u) du - \int_{-\infty}^0 (-u)^{H-1/2} \xi_B(u) du \right] \\
 &= h^H [x(\tau + t) - x(\tau)],
 \end{aligned} \tag{10}$$

which completes the proof that FBM is self-similar.

APPENDIX B.

MEAN SQUARED SEPARATION OF BRANCHING TRAJECTORIES

Consider two branching discrete FBM trajectories, x_t and x'_t ,

$$\begin{aligned} x_t &= \sum_{i=1}^t \xi_i \\ x'_t &= \sum_{i=1}^t \xi'_i \end{aligned} \quad (1)$$

where x_t is the parent trajectory and x'_t is the child trajectory that branched at time $t = t_b$.

As implied by Eq. 2.16, the MSD can be written

$$\begin{aligned} \langle (x_t - x_{t_0})^2 \rangle &= \sum_{i,j=t_0+1}^t \langle \xi_i \xi_j \rangle \\ &= \sigma^2 (t - t_0)^{2H}, \end{aligned} \quad (2)$$

where σ^2 is the variance of the step length.

The mean squared separation (MSS) between the parent and child at time t is

$$\begin{aligned} \langle \Delta x_t^2 \rangle &= \langle (x_t - x'_t)^2 \rangle \\ &= \sum_{i,j=1}^t \langle \xi_i \xi_j \rangle + \sum_{i,j=1}^t \langle \xi'_i \xi'_j \rangle - 2 \sum_{i,j=1}^t \langle \xi_i \xi'_j \rangle \end{aligned} \quad (3)$$

Each sum can be split across the branch time t_b like

$$\sum_{i,j=1}^t \langle \xi_i \xi_j \rangle = \sum_{i=1}^{t_b} \sum_{j=1}^{t_b} \langle \xi_i \xi_j \rangle + \sum_{i=1}^{t_b} \sum_{j=t_b+1}^t \langle \xi_i \xi_j \rangle + \sum_{i=t_b+1}^t \sum_{j=1}^{t_b} \langle \xi_i \xi_j \rangle + \sum_{i=t_b+1}^t \sum_{j=t_b+1}^t \langle \xi_i \xi_j \rangle, \quad (4)$$

and the sums containing only ξ or ξ' can exchange their bounds and be simplified to

$$\begin{aligned} \sum_{i,j=1}^t \langle \xi_i \xi_j \rangle &= \sum_{i=1}^{t_b} \sum_{j=1}^{t_b} \langle \xi_i \xi_j \rangle + 2 \sum_{i=1}^{t_b} \sum_{j=t_b+1}^t \langle \xi_i \xi_j \rangle + \sum_{i=t_b+1}^t \sum_{j=t_b+1}^t \langle \xi_i \xi_j \rangle \\ &= \sigma^2 [t_b^{2H} + (t - t_b)^{2H}] + 2 \sum_{i=1}^{t_b} \sum_{j=t_b+1}^t \langle \xi_i \xi_j \rangle. \end{aligned} \quad (5)$$

In addition, since $\xi_t = \xi'_t$ for all $t \leq t_b$, the cross-term sum can be written

$$\sum_{i,j=1}^t \langle \xi_i \xi'_j \rangle = \sigma^2 t_b^{2H} + \sum_{i=1}^{t_b} \sum_{j=t_b+1}^t \langle \xi'_i \xi'_j \rangle + \sum_{i=t_b+1}^t \sum_{j=1}^{t_b} \langle \xi_i \xi_j \rangle + \sum_{i=t_b+1}^t \sum_{j=t_b+1}^t \langle \xi_i \xi'_j \rangle \quad (6)$$

Plugging these back into the MSS:

$$\begin{aligned} \langle \Delta x_t^2 \rangle &= 2\sigma^2 [t_b^{2H} + (t - t_b)^{2H}] + 2 \sum_{i=1}^{t_b} \sum_{j=t_b+1}^t \langle \xi_i \xi_j \rangle + 2 \sum_{i=1}^{t_b} \sum_{j=t_b+1}^t \langle \xi'_i \xi'_j \rangle \\ &\quad - 2 \left(\sigma^2 t_b^{2H} + \sum_{i=1}^{t_b} \sum_{j=t_b+1}^t \langle \xi'_i \xi'_j \rangle + \sum_{i=t_b+1}^t \sum_{j=1}^{t_b} \langle \xi_i \xi_j \rangle + \sum_{i=t_b+1}^t \sum_{j=t_b+1}^t \langle \xi_i \xi'_j \rangle \right) \quad (7) \\ &= 2\sigma^2 (t - t_b)^{2H} - 2 \sum_{i=t_b+1}^t \sum_{j=t_b+1}^t \langle \xi_i \xi'_j \rangle. \end{aligned}$$

For the half-loss and full-loss models, it is intuitively clear that the two trajectories will not be correlated with one another after the branch ($\langle \xi_i \xi'_j \rangle = 0$), as one or both will have forgotten about their shared history, so the MSS will be simply $\langle \Delta x_t^2 \rangle = 2\sigma^2 (t - t_b)^{2H}$. For the no-loss model, however, it is difficult to make a strong statement about how the two trajectories will be correlated after the branch. It seems likely that the two trajectories will be correlated to one another after the branch since they are both correlated to a shared history, but the exact mathematical form of these correlations is not easily intuited. The observed correlations following a branch in the no-loss model are examined in Sec. 3.2

What is here called the no-loss model of bFBM was studied in mathematical detail in Ref. [22] using continuous-time FBM, where the covariance of branching trajectories was found to be

$$\langle x(t)x'(t) \rangle = \sigma^2 t^{2H} - \sigma^2 (t - t_b)^{2H} \frac{2^{2H-1} \sqrt{\pi}}{\Gamma(1-H)\Gamma(H+1/2)}, \quad (8)$$

where Γ is the gamma function. The MSS is then

$$\begin{aligned}\langle \Delta x^2(t) \rangle &= \langle x^2(t) \rangle + \langle x'^2(t) \rangle - 2 \langle x(t)x'(t) \rangle \\ &= \sigma^2(t - t_b)^{2H} \frac{2^{2H} \sqrt{\pi}}{\Gamma(1 - H)\Gamma(H + 1/2)}.\end{aligned}\tag{9}$$

However, as previously stated, this result applies to continuous-time bFBM where trajectories have infinitely long memory, so it is not necessarily expected to hold in simulations of discrete bFBM where trajectories are computationally restricted to a finite memory.

APPENDIX C.

STEP CORRELATIONS AFTER BRANCHING IN NO-LOSS MODEL

Consider two branching continuous-time FBM trajectories, x and x' , that branched from each other at time t_b in the no-loss model. The increments of x and x' are

$$\begin{aligned}\xi(t) &= x(t + \delta t) - x(t) \\ \xi'(t) &= x'(t + \delta t) - x'(t),\end{aligned}\tag{1}$$

for constant $\delta t > 0$. The (simultaneous) correlations between steps ξ and ξ' at time t can be written

$$\begin{aligned}\langle \xi(t)\xi'(t) \rangle &= \langle [x(t + \delta t) - x(t)][x'(t + \delta t) - x'(t)] \rangle \\ &= \langle x(t + \delta t)x'(t + \delta t) \rangle - \langle x(t + \delta t)x'(t) \rangle - \langle x(t)x'(t + \delta t) \rangle + \langle x(t)x'(t) \rangle \\ &= \langle x(t + \delta t)x'(t + \delta t) \rangle - 2\langle x(t + \delta t)x'(t) \rangle + \langle x(t)x'(t) \rangle,\end{aligned}\tag{2}$$

where, by symmetry, $\langle x(t + \delta t)x'(t) \rangle = \langle x(t)x'(t + \delta t) \rangle$.

In their study of continuous-time bFBM, Casanova and Igelbrink [22] found the covariance of two branching trajectories at times $t_1 > t_b$ and $t_2 > t_b$ to be

$$\begin{aligned}\langle x(t_1)x'(t_2) \rangle &= K_H \left\{ \int_{-\infty}^0 \left[(t_1 - s)^{H-1/2} - (-s)^{H-1/2} \right] \left[(t_2 - s)^{H-1/2} - (-s)^{H-1/2} \right] ds \right. \\ &\quad \left. + \int_0^{t_b} (t_1 - s)^{H-1/2} (t_2 - s)^{H-1/2} ds \right\},\end{aligned}\tag{3}$$

where K_H is a constant that ensures $\langle \xi^2(t) \rangle = 1$, which Casanova and Igelbrink determine to be

$$K_H = -\frac{2^{2H}\sqrt{\pi}}{\Gamma(-H)\Gamma(H+1/2)},\tag{4}$$

where Γ is the gamma function.

Plugging Eq. (3) into Eq. (2) yields

$$\begin{aligned} \langle \xi(t)\xi'(t) \rangle = & K_H \left(\int_{-\infty}^0 \left\{ \left[(t + \delta t - s)^{H-1/2} - (-s)^{H-1/2} \right]^2 + \left[(t - s)^{H-1/2} - (-s)^{H-1/2} \right]^2 \right. \right. \\ & \left. \left. - 2 \left[(t + \delta t - s)^{H-1/2} - (-s)^{H-1/2} \right] \left[(t - s)^{H-1/2} - (-s)^{H-1/2} \right] \right\} ds \right. \\ & \left. + \int_0^{t_b} \left[(t + \delta t - s)^{2H-1} + (t - s)^{2H-1} - 2(t + \delta t - s)^{H-1/2}(t - s)^{H-1/2} \right] ds \right) \end{aligned} \quad (5)$$

Both integrands can be factored into $[(t + \delta t - s)^{H-1/2} - (t - s)^{H-1/2}]^2$, so the correlations are thus

$$\langle \xi(t)\xi'(t) \rangle = K_H \int_{-\infty}^{t_b} \left[(t + \delta t - s)^{H-1/2} - (t - s)^{H-1/2} \right]^2 ds. \quad (6)$$

The above integral cannot be solved exactly, nor can the dependence on t and t_b be extracted from the integral. Seeking an approximate solution, consider the case where $t \gg \delta t$. Taylor expanding the integrand to second order about $\delta t = 0$ yields

$$\left[(t + \delta t - s)^{H-1/2} - (t - s)^{H-1/2} \right]^2 \approx \delta t^2 \left(H - \frac{1}{2} \right)^2 (t - s)^{2H-3}. \quad (7)$$

Integrating this approximate expression gives

$$\langle \xi(t)\xi'(t) \rangle \approx -K_H \delta t^2 \frac{(H - 1/2)^2}{2H - 2} (t - t_b)^{2H-2} \quad (8)$$

Using Eq. (4) and the gamma function's fundamental property $\Gamma(x + 1) = x\Gamma(x)$, the approximate step correlations can be simplified to

$$\langle \xi(t)\xi'(t) \rangle \approx \delta t^2 (t - t_b)^{2H-2} \frac{2^{2H}(H - 1/2)\sqrt{\pi}}{(2H - 2)\Gamma(-H)\Gamma(H - 1/2)}. \quad (9)$$

Note that $H - 1/2$ and $\Gamma(H - 1/2)$ have the same sign, as do $2H - 2$ and $\Gamma(-H)$, given that $0 < H < 1$. In addition, $\langle \xi(t)\xi'(t) \rangle$ vanishes when $H = 1/2$ (i.e. Brownian motion). This means that when $H \neq 1/2$, the steps of two branching trajectories are positively correlated for all times after the branch.

REFERENCES

- [1] T. Vojta, S. Halladay, S. Skinner, S. Janušonis, T. Guggenberger, and R. Metzler, *Phys. Rev. E* **102**, 032108 (2020).
- [2] S. Janušonis, N. Detering, R. Metzler, and T. Vojta, *Front. Comput. Neurosci.* **14**, 56 (2020).
- [3] M. Hingorani, A. Viviani, J. Sanfilippo, and S. Janušonis, *Front. Neurosci.* **16**, 994735 (2022).
- [4] Y. Numasawa, T. Hattori, S. Ishiai, Z. Kobayashi, T. Kamata, M. Kotera, S. Ishibashi, N. Sanjo, H. Mizusawa, and T. Yokota, *J. Affect. Disord.* **213**, 191 (2017).
- [5] G. H. Maia, J. I. Soares, S. G. Almeida, J. M. Leite, H. X. Baptista, A. N. Lukoyanova, C. S. Brazete, and N. V. Lukoyanov, *Brain Res. Bull.* **152**, 95 (2019).
- [6] S. Janušonis and N. Detering, *Biochimie* **161**, 15 (2019).
- [7] S. Janušonis, J. H. Haiman, R. Metzler, and T. Vojta, *Front. in Comput. Neurosci.* **17**, 1189853 (2023).
- [8] R. Brown, *Philos. Mag.* **4**, 161 (1828).
- [9] A. Einstein, *Investigations on the Theory of the Brownian Movement* (Dover, 1956).
- [10] F. C. Klebaner, *Introduction to Stochastic Calculus With Applications* (Imperial College Press, 2012).
- [11] R. Kubo, *Rep. Progr. Phys.* **29**, 255 (1966).
- [12] R. Metzler, J.-H. Jeon, A. Cherstvy, and E. Barkai, *Phys. Chem. Chem. Phys.* **16**, 24128 (2014).
- [13] T. Guggenberger, G. Pagnini, T. Vojta, and R. Metzler, *New J. Phys.* **21**, 022002 (2019).
- [14] A. H. O. Wada and T. Vojta, *Phys. Rev. E* **97**, 020102 (2018).
- [15] P. Lévy, *Random functions: general theory with special reference to Laplacian random functions*, Vol. 1 (University of California Press, 1953).
- [16] A. N. Kolmogorov, *Acad. Sci. URSS (N. S.)* **26**, 115 (1940).
- [17] B. B. Mandelbrot and J. W. Van Ness, *SIAM Review* **10**, 422 (1968).
- [18] H. Qian, in *Processes with Long-Range Correlations*, Lecture Notes in Physics, Vol. 621, edited by G. Rangaran and M. Ding (Springer, 2003) p. 22.
- [19] H. A. Makse, S. Havlin, M. Schwartz, and H. E. Stanley, *Phys. Rev. E* **53**, 5445 (1996).

- [20] J. R. M. Hosking, *Water Resour. Res.* **20**, 1898 (1984).
- [21] R. J. Adler and G. Samorodnitsky, *The Annals of Probability* **23**, 743 (1995).
- [22] A. G. Casanova and J. L. Igelbrink, (2023), arXiv:2310.04386 .
- [23] G. Marsaglia, “Double precision RNGs”, posted to sci.math.num-analysis (2005).
- [24] E. G. Coffman, Jr., M. R. Garey, and D. S. Johnson, *SIAM Journal on Computing* **7**, 1 (1978).
- [25] A. Rayle, J. House, R. Beattie-Hauser, G. Khairnar, S. Janušonis, R. Metzler, and T. Vojta, (to be published) (2024).

VITA

Reece Beattie-Hauser was born in St. Louis, Missouri in 2001, the youngest of three brothers. He graduated from Lafayette High School in the class of 2019 and continued his education at the Missouri University of Science & Technology, pursuing a bachelor's degree in Physics. He began working as a student research assistant for Thomas Vojta in the summer of 2020, studying magnetic phase transitions in diluted systems. He enrolled in the Physics department's Grad Track Pathway program, earning his bachelor's degree in May 2023 and immediately enrolling as a master's student the following summer semester. He received his master's degree in Physics in May 2024.